Analysis of the sub-barrier fusion of $^{16}O + ^{148,150,152,154}Sm$

R. G. Stokstad* and E. E. Gross
Oak Ridge National Laboratory, Oak Ridge, Tennessee 37830
(Received 18 August 1980)

Recent measurements of the sub-barrier fusion of ^{16}O with isotopes of Sm, which span the transition region from spherical to deformed equilibrium shapes, are analyzed in terms of static and dynamic reaction models. The classical equivalent-spheres method of incorporating the effect of nuclear deformation on heavy-ion fusion is shown to overpredict the experimentally observed differences in the fusion cross sections. An approximate, classical estimate of dynamic effects connected with the rotation of the target before fusion removes part, but not all, of this discrepancy. Coupled-channels calculations, which treat dynamic effects through the excitation of the 2^+ and 4^+ levels, are also presented. An estimate is given of the effects one may expect to observe for fusion with a polarized deformed target.

[NUCLEAR REACTIONS Barrier-penetration analysis of σ_{fusion} for $^{16}O + ^{148,150,152,154}Sm$, $E_{lab} = 60$–75 MeV, including effects of static deformation. Consideration of dynamic effects. Coupled-channels analysis.]

I. INTRODUCTION

When interest in heavy-ion-induced reactions first developed nearly 30 years ago, it was recognized that the deformability of nuclei could have consequences for the fusion of heavy ions.[1] Repulsive Coulomb forces were expected to induce an oblate deformation, with the axis of symmetry along the line connecting the centers of the colliding nuclei, resulting in an effective increase in the barrier for fusion. The possible existence of superheavy nuclei and the hope that they might be produced by the fusion of heavy ions stimulated further theoretical examination of this subject.[2] Studies by Wong[3] using the adiabatic approximation and by a number of authors who also considered the dynamics of the collision[4-6] indicated that the observable effects of induced deformation were expected to be much smaller than originally estimated by Beringer.[2] To this day, the effect on the fusion cross section of Coulomb-induced distortions of the nuclear surface has not been clearly identified or isolated in an experiment. This may be a consequence both of the small size of the predicted effect and of other effects involving deformation which can be much larger.

Many nuclei possess an equilibrium deformation. We refer to this as static deformation, in contrast to the induced deformation discussed above. In their work on fission, Hill and Wheeler[7] pointed out that the barrier for α-particle emission from a deformed nucleus should depend on the angle of emission with respect to the axis of the symmetry. Experiments on the angular distribution of α particles emitted by oriented ^{237}Np nuclei[8] verified that emission in the direction of the angular momentum vector was favored. Since the angular momentum of the ground state is expected to be collinear with the axis of symmetry of the prolate ^{237}Np nucleus, this experiment suggested that the barrier for emission from the polar region is, indeed, lowered. Recently, Beckerman and Blann[9] have drawn attention to the possible importance of deformation for the emission of light particles from high-spin states in nuclei. Rapidly rotating nuclei are expected to be highly deformed, which in turn should influence the transmission coefficients for particle emission as well as the barrier for fission.

The consequences of the above considerations for the inverse reaction, the scattering, and the capture of α particles by deformed nuclei were examined by Rasmussen and Sugawara-Tanabe.[10] Integration of the barrier penetrability over all the angles of orientation for an unpolarized target results in an increase in the fusion cross section for deformed nuclei, which is pronounced at sub-Coulomb bombarding energies. Thus, the effective barrier is lowered, or, equivalently, the effective capture radius is increased as a result of static deformation. (The effects of static deformation are expected to be much larger than those for Coulomb-induced deformation.) Early measurements of heavy-ion fusion cross sections for $^{40}Ar + ^{164}Dy$ (Ref. 11) and for $^{84}Kr + ^{72}Ge$, ^{116}Cd (Ref. 12) indicated barrier radii of 1.45 $(A_1^{1/3} + A_2^{1/3})$ and 1.32 $(A_1^{1/3} + A_2^{1/3})$ for the deformed and spherical systems, respectively. Wong[13,14] has incorporated the effect of static deformation in the analyses of a number of heavy-ion-induced reactions.

Several experiments have been designed specifically to reveal the effects of deformation on the fusion cross section. Freiesleben and Huizen-

ga[15] measured the fusion fission of ^{4}He+ ^{233,238}U at sub-barrier energies and compared it with similar measurements[16] for ^{4}He+ ^{208}Pb, ^{209}Bi. On the basis of the observed *energy dependence*, they did not find any evidence for the effect of deformation, even though the cross sections extended over five orders of magnitude. Alexander *et al.*[17] reexamined these data from the point of view of the *magnitude* of the cross sections. They fit the data for ^{4}He+ ^{208}Pb and used this to predict the fusion cross section for ^{4}He+ ^{238}U under the assumption that ^{238}U is spherical. This prediction resulted in an underestimate of the observed cross section for ^{238}U. No quantitative prediction based on the known deformation of ^{238}U was made, however.

The reactions of ^{35}Cl with the even isotopes of Ni have been studied by Scobel *et al.*[18] for $E_{\rm lab}$ = 91–170 MeV. The deformations of the Ni isotopes, derived from the $B(E2)$ value assuming a rigid-rotor model, vary from $\beta_2 = +0.18$ to ~ -0.2 for ^{58}Ni to ^{64}Ni. They used the "equivalent-spheres" formalism of Wong[14] to analyze their results and found that fits to the data were much improved when deformation was taken into account.

Vaz and Alexander[19,20] have made systematic analyses of fusion and total reaction cross sections. They incorporate a spectrum of barrier heights having a uniform distribution varying from $E_0 - \Delta$ to $E_0 + \Delta$ in the expression[14] for the penetration of a spherically symmetric parabolic potential. Values of Δ ranging from ~2 to ~8 MeV were deduced. Since both the effect of deformation and the inadequacy of a parabolic approximation for the barrier could influence the value of Δ, it is difficult to conclude that the experimental data they have analyzed *demonstrate* the effects of deformation. It is interesting to note, however, that the system ^{40}Ca+ ^{32}S, involving a doubly magic nucleus, had the smallest value of Δ (2.2 MeV), while the system ^{20}Ne+ ^{238}U, in which both target and projectile are strongly deformed, had the largest value of Δ (7.7 MeV).

The fusion of the doubly magic system ^{48}Ca + ^{208}Pb has been studied recently by Morrissey *et al.*[21] A comparison[21] of the cross sections for this system with ^{40}Ar+ ^{238}U and ^{40}Ar+ ^{165}Ho as a function of the ratio of bombarding energy to barrier height suggests relatively lower cross sections for the fusion of spherical nuclei.

Even though the above studies strongly suggest that the effect of deformation on heavy-ion fusion is measurable and has been observed, it was felt that some of the ambiguities and difficulties associated with these earlier studies might be reduced by additional experiments. In particular, the choice of a spherical projectile, a series of targets of the same element whose isotopes vary from vibrational to strongly deformed, and an experimental technique allowing precision measurements far below the barrier would offer many advantages. Such experiments on the fusion of ^{16}O+ ^{148,150,152,154}Sm have been reported by Stokstad *et al.*[22] This article describes an analysis of these results. Given the precision of the cross sections for fusion, $\sigma_{\rm fus}$, and the known structural characteristics of the Sm isotopes, it becomes possible not only to establish more clearly the effect of deformation, but also to *test* the various methods which have been put forth to calculate $\sigma_{\rm fus}$ for deformed nuclei. Recently, experimental data of similar quality for the fusion of ^{40}Ar + ^{144,148,154}Sm have become available. These results are described in a separate publication.[23]

Section II describes the analysis of the data in terms of the usual equivalent-spheres approximation and discusses possible reasons for its failure. In Sec. III, calculations with a single averaged spherical potential are described. Classical estimates of dynamical effects are discussed briefly in Sec. IV. Coupled-channels analyses, which include both static and dynamic effects, are presented in Section V. A summary and conclusions are contained in the last section, and an appendix describes effects that might be observable in an experiment using a polarized target.

II. EQUIVALENT-SPHERES ANALYSIS

The equivalent-spheres approximation treats the fusion of a spherical projectile with a deformed nucleus by replacing the latter with a series of spherical nuclei of different radii. The radius of a given sphere depends on the angle of orientation, θ, of the axis of symmetry of the deformed target nucleus with respect to the initial direction of the projectile through the equation

$$R_t(\theta) = R_t[1 + \Sigma_\lambda \beta_\lambda Y_\lambda^0(\theta)]. \quad (1)$$

The parameters $\beta_\lambda (\lambda = 2, 4, 6, \ldots)$ and spherical harmonic functions $Y_\lambda^0(\theta)$ describe the deviation of the nuclear surface from a sphere with radius R_t^0. Since it is the shift of the nuclear surface that is the relevant quantity and since this shift is proportional to $\beta_\lambda R_t^0$, all values of β_λ given in this paper are normalized to correspond to a standard radius given by $1.2\, A_t^{1/3}$ fm, where A_t is the atomic mass (u) of the target nucleus.

Before considering the effects of deformation, it is essential to be able to make a proper description of the fusion of spherical nuclei. In principle, this could be done by calculating the nuclear potential for the collision of two spheres using, e.g , the proximity formulation,[24] a folding mod-

el,[25] or empirical formulations.[26,27] In practice, this is not possible because the cross sections at sub-barrier energies are extremely sensitive to slight changes in the radius or strength of the nuclear potential. Thus, the use of a potential *a priori* could introduce errors which would be comparable to or larger than the effects of deformation. This problem is solved by empirically determining a potential to describe sub-barrier fusion cross sections for a system which is spherical and yet otherwise similar to the deformed system. An *approximation* to this ideal situation is found in the samarium isotopes which, in the neutron-deficient region, exhibit vibrational characteristics (^{144,148}Sm) and become strongly deformed as the neutron number reaches and exceeds 90 (^{152,154}Sm).

The result of a search for a spherical potential which reproduces the excitation function for the fusion of ^{16}O+^{148}Sm is shown in Fig. 1. The fusion cross sections shown here were calculated by solving the Schrödinger equation for a *complex* potential and equating the fusion cross section with the total absorption cross section. The potentials used here would not reproduce the elastic scattering and thus are not "optical model" potentials. This procedure effectively removes from explicit consideration all processes which cannot be described solely by the penetration of a real, one-dimensional barrier (e.g., neck formation[23])

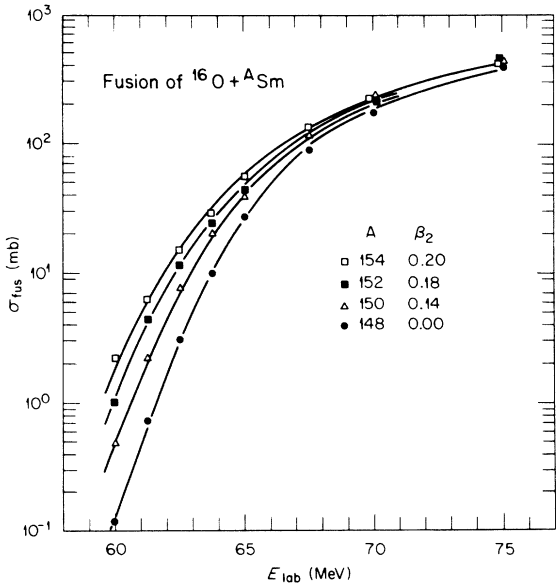

FIG. 1. Cross sections for the fusion of ^{16}O+^{148,150,152,154}Sm (Ref. 22). The full curves are fits to the data as described in the text for the indicated values of β_2.

and makes it possible to focus on effects having to do with the nuclear structure of the target.

The real part of the nuclear potential has a liquid-drop form factor,[27]

$$V_n(r) = V_0 \exp[(R-r)/d], \quad r > R$$
$$= V_0, \quad r \leq R, \tag{2}$$

$$R = r_0(A_p^{1/3} + A_t^{1/3}). \tag{3}$$

A Woods-Saxon form factor was used for the imaginary potential

$$W(r) = W_0\left[1 + \exp\left(\frac{r-R_i}{a_i}\right)\right]^{-1}, \tag{4}$$

for which $R_i = r_i(A_p^{1/3} + A_t^{1/3})$.

The values of the reduced parameters which fit the data for ^{16}O+^{148}Sm by assuming $\beta_2 = 0.0$ are labeled as case (i) in Table I. As was found for the systems in Ref. 27, the radii are smaller and the diffusivities larger (in Table I) than those values which would describe the elastic scattering (see Sec. V). Note that the imaginary potential approximates a square well. The above real (nuclear plus Coulomb) and imaginary spherical potentials are shown in Fig. 2 (labeled by $\beta_\lambda = 0$) for the case of ^{16}O+^{154}Sm. The imaginary potential is seen to extend slightly beyond the point where the real potential reaches its maximum. The energy dependence of σ_{fus} depends sensitively on the location of the imaginary potential.

The calculation of the fusion cross section for a spherical projectile of radius R_p and a deformed target aligned at an angle θ is done by solving the Schrödinger equation for the real potential,

$$V[R(\theta), r] = V_n[R(\theta), r] + V_C[R(\theta), r], \tag{5}$$

$W = W[R_i(\theta), r]$, where $R(\theta) = R_p + R_t(\theta)$ and $R_t(\theta)$ is given by Eq. (1). A similar expression gives the imaginary radius $R_i(\theta)$. The real and imaginary potentials are assumed to be described by the same deformation parameters. The Coulomb potential V_C also depends on the deformation and orientation of the target nucleus. For a nucleus described by Eq. (1), we have used

$$V_C[R(\theta), r] = \sum_{\lambda=\text{even}} V_{C\lambda},$$

where

$$V_{C0}(r) = \frac{Z_1 Z_2 e^2}{r},$$

$$V_{C2}(r) = \frac{V_{C0}(r)}{r^2}\left(\frac{9}{20\pi}\right)^{1/2}\beta_2 P_2(R_t^0)^2 + \frac{3}{7\pi}(\beta_2 P_2 R_t^0)^2,$$

$$V_{C4}(r) = \frac{V_{C0}(r)}{r^4}\frac{9}{28\pi}[\beta_2 P_2(R_t^0)^2]^2 + \frac{1}{\sqrt{4\pi}}\beta_4 P_4(R_t^0)^4,$$

$$V_{C6}(r) = \frac{V_{C0}(r)}{r^6}\left(\frac{9}{52\pi}\right)^{1/2}\beta_6 P_6(R_t^0)^6,$$

TABLE I. Parameters of the real and imaginary potentials.

	β_2 (^{148}Sm)	V_0 (MeV)	r_0 (fm)	d (fm)	W_0 (MeV)	r_i (fm)	a_i (fm)
(i) [a]	0	−36.0	0.986	2.13	10.0	1.295	0.026
(ii) [a]	0.10	−36.0	1.015	1.98	10.0	1.274	0.079
(iii) [a]	0.13	−36.0	0.994	2.19	10.0	1.19	0.165
(iv) [b]	0	50	1.09	1.35	17.5	1.34	0.069

[a]The real potential has a liquid-drop form factor (Ref. 27) [Eq. (2)]. The imaginary potential has a Woods-Saxon form factor.

[b]Both real and imaginary potentials have a Woods-Saxon form factor.

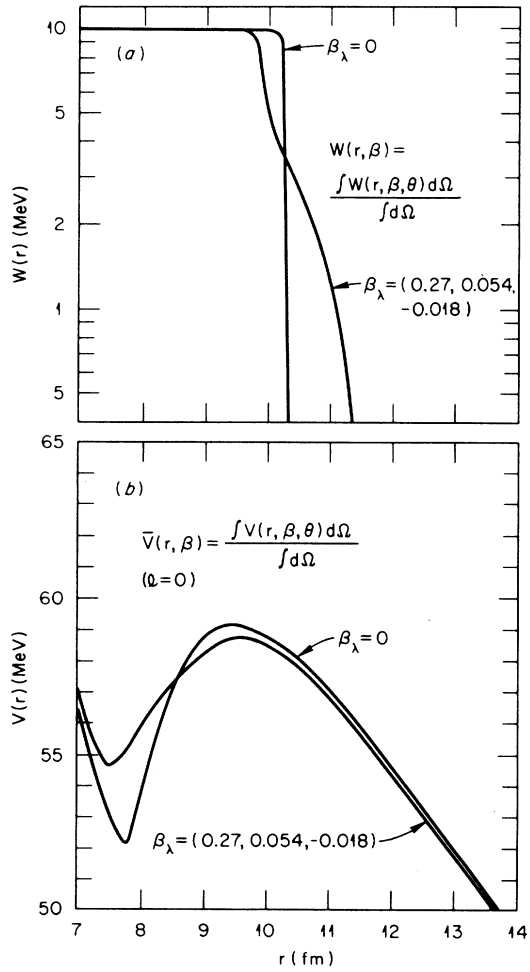

FIG. 2. The potentials obtained from fitting the data. (a) The spherical imaginary potential ($\beta_\lambda = 0$), shown here for ^{16}O+^{154}Sm, as obtained from fitting the data for ^{16}O+^{148}Sm with $\beta_2 = 0$. The radial dependence obtained after deforming the potential and averaging it over all orientations is also shown. (b) As above, but for the real, Coulomb-plus-nuclear potential.

and the P_λ are the Legendre polynomials.[6,14,28]

For radii $r < R_m$, where $R_m = 1.25\,(A_p^{1/3} + A_t^{1/3})$fm is the Coulomb matching radius, the following expression for the Coulomb potential was used:

$$V_C(r) = \left[\frac{2\lambda+3}{\lambda+1} - \left(\frac{r}{R_m}\right)^{\lambda+2}\right]\frac{\lambda+1}{\lambda+2} V_{C\lambda}(R_m), \quad r < R_m. \quad (6)$$

This formula has a continuous first derivative at $r = R_m$ and for $\lambda = 0$ is the expression for a point charge and a uniformly charged sphere usually used in optical model codes. The calculated cross sections are not very sensitive to the precise form of Eq. (6) nor to reasonable variations in the value of R_m.

The dependence of the real potential on the angle of orientation is illustrated in Fig. 3 for ^{16}O+^{154}Sm; the deformation parameters used here to describe ^{154}Sm are $\beta_\lambda = (0.27,\ 0.054,\ -0.018)$ for $\lambda = 2,\ 4,\ 6$, respectively.[29] Note that the height of the barrier increases by about 9 MeV as θ varies from 0 to 90 degrees. The potential for $\theta = 52.5°$ corresponds very closely to the spherical case. The consequences of these different barrier heights for the fusion cross section at a bombarding energy of 54.3-MeV c.m. (60-MeV lab) are shown in Fig. 4. Here, the equivalent-spheres cross section is shown as a function of the angle of orientation and is seen to vary by over three orders of magnitude.

The fusion cross sections shown in Fig. 4 have to be averaged over all angles of orientation since the target nucleus is not aligned. This average is written

$$\sigma_{fus} = \int_0^{\pi/2} \sigma_{fus}(\theta) \sin\theta\, d\theta \quad (7)$$

and has been evaluated numerically. The fusion cross section weighted by the solid angle factor $\sin\theta$ is also shown in Fig. 4 and is a maximum

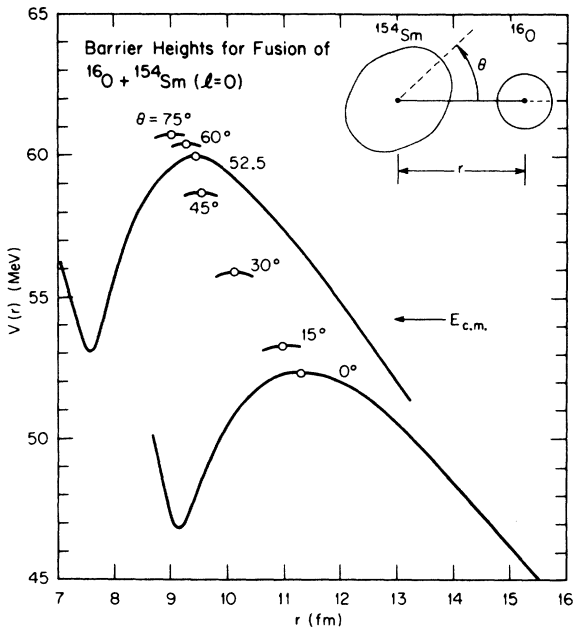

FIG. 3. The different barriers associated with different angles of orientation, calculated in the equivalent-spheres approximation. The lowest energy at which a measurement was made (60-MeV lab) is indicated.

for a 15° angle of inclination.

An indication of the calculated sensitivity of σ_{fus} to the magnitude of the deformation is given in Fig. 5. The ratio of the σ_{fus} for the deformed and spherical cases is plotted *versus* the quadrupole deformation parameter β_2. A change in deformation from 0 to 0.3 causes a change of more than an order of magnitude in σ_{fus}. This sensitivity is a consequence of the small barrier penetrability at this low bombarding energy. The lack of symmetry about $\beta = 0$ is a result of the asymmetry of the second Legendre polynomial.

Once the complex spherical potential has been determined by fitting $^{16}O + ^{148}Sm$ with $\beta_\lambda = 0$, values of β may be deduced for the other Sm isotopes by fitting the measured excitation functions for σ_{fus}. In this procedure, the reduced radii r_0 and r_i and diffusivities d and a_i are held constant, V_0 and W_0 are constant, and the only changes in the spherical potential arise through the $A^{1/3}$ dependence of the radius. Such fits to the data are shown by the full curves in Fig. 1 and have been obtained for values of $\beta_2 = 0.0$, 0.14, 0.18, and 0.20 for $^{148,150,152,154}Sm$, respectively. Since β_2 is treated as a free parameter, the values of β_4 and β_6 were set equal to zero. Figure 6 compares these deduced values of β_2 [curve (a)] with values determined from α-particle scattering,[29-32] from transitions in μ-mesic atoms,[33] and from reduced $E2$ transition matrix elements.[34,35] In the latter case, β_2 is defined by[34,35]

$$\beta_2 = [B(E2, 0 \rightarrow 2)]^{1/2}[3ZR_t^2/4\pi]^{-1},$$

where $R_t = 1.2\, A_t^{1/3}$.

The above procedure for determining the deformation of a nucleus through an analysis of a fusion excitation function does not yield results in agreement with other methods for determining

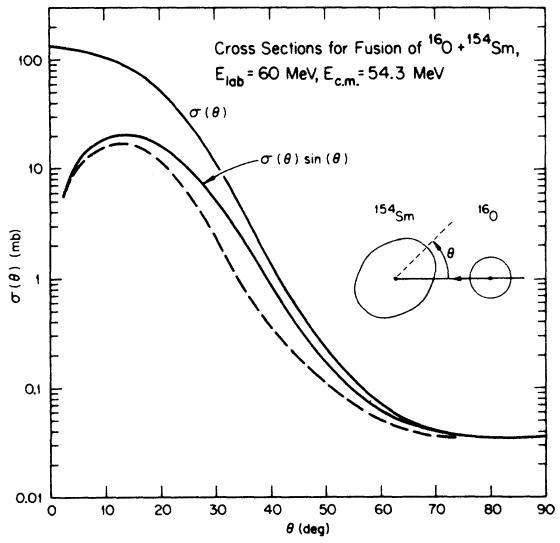

FIG. 4. The dependence of the calculated fusion cross section on the angle of orientation. The dashed line shows the value of $\sigma(\theta)\sin\theta$ if the target nucleus is allowed to rotate (under the influence of an electric quadrupole moment) until the distance of closest approach is obtained.

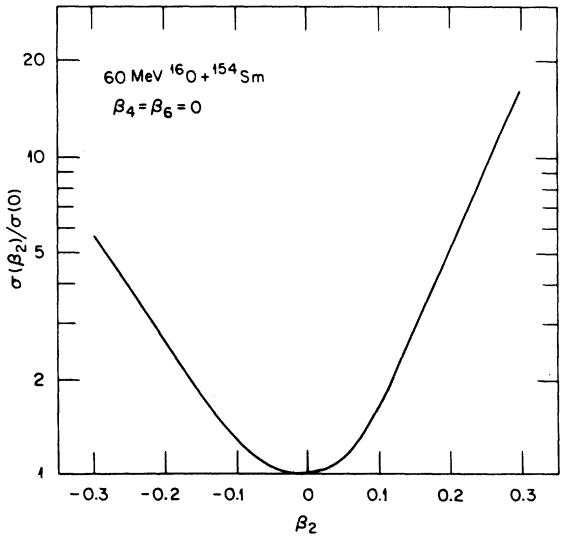

FIG. 5. The predicted relative change in the fusion cross section as a function of β_2.

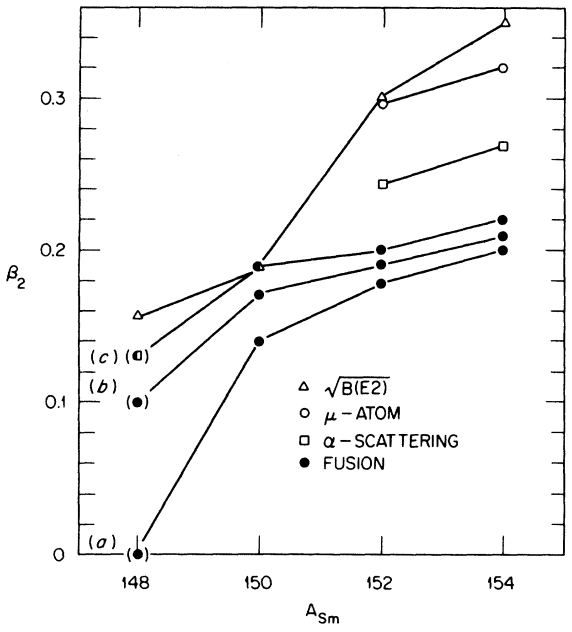

FIG. 6. Comparison of the values of β_2 deduced from fitting σ_{fus} with those deduced by other methods.

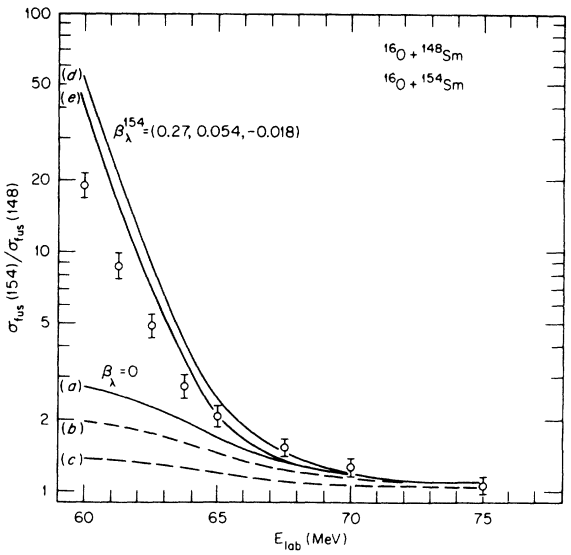

FIG. 7. Measured and predicted ratios of the fusion cross sections for $^{16}O + ^{154}Sm$ and $^{16}O + ^{148}Sm$. The predictions [curves (a)–(e)] are discussed in the text.

the deformation. Although the values deduced from fusion shown in Fig. 6 exhibit the correct trend with the mass of the samarium isotopes, the quantitative discrepancies are well outside the range of experimental error. (Similar conclusions were reached in the case of ^{40}Ar fusing with $^{144,148,154}Sm$, Ref. 23.) In the remainder of this section, we will examine a number of possible reasons for these discrepancies.

The results shown in Fig. 6 for curve (a) immediately suggest that the difficulty might be with the assumption that ^{148}Sm is spherical, i.e., that $\beta_2 = 0$. The fact that ^{148}Sm exhibits a vibrational-like energy spectrum implies that the time-averaged value of β_2 is zero. The value of β_2 deduced from the $B(E2)$ value (by assuming a rotational model) and from α-particle inelastic scattering[30] represents, effectively, a root-mean-square (rms) value of a fluctuating quantity. Thus, while in its excited 2^+ state and through zero-point motion while in its ground state,[36] the ^{148}Sm nucleus can be momentarily deformed. An approximate way of treating this situation is to assign a permanent deformation to ^{148}Sm. This produces a distribution of barrier heights (see Fig. 3) just as a fluctuating value of β_2 produces a distribution of barrier heights. (These distributions are not necessarily the same, however.)

The values of β_2 indicated by curves (b) and (c) in Fig. 6 result when the fitting procedure is repeated as above, except that finite deformations of $\beta_2 = 0.10$ and $\beta_2 = 0.13$ are assumed for ^{148}Sm.

The spherical potential, which is determined by fitting the data for $^{16}O + ^{148}Sm$ under this assumption, is of course dependent on the assumed value of β_2. [The parameters describing these potentials are given in Table I as cases (ii) and (iii).] While the use of a finite value of β_2 results in somewhat larger deduced values of β_2 for $^{150,152,154}Sm$, as may be seen in Fig. 6, significant discrepancies still remain with values of β_2 derived from other measurements.

The extent of the discrepancy between an analysis based on the equivalent-spheres approximation and the experimental results is demonstrated by predicting σ_{fus} for $^{16}O + ^{154}Sm$ using the known deformation parameters for ^{154}Sm: $\beta_2 = 0.27$, $\beta_4 = 0.054$, $\beta_6 = -0.018$ (Ref. 29). These values for β_2 and β_4 agree well with other measurements and analyses of α-particle inelastic scattering.[31,32] In the following, it is sufficient to consider only the differences between $^{16}O + ^{148}Sm$ and $^{16}O + ^{154}Sm$, which we express as the ratio $\sigma_{fus}(154)/\sigma_{fus}(148)$ and show in Fig. 7. Curve (a), labeled $\beta_\lambda = 0$, is the ratio which would be expected if ^{154}Sm were spherical [as has been assumed for ^{148}Sm, case (i) in Table I] but with a larger radius given by an $A^{1/3}$ dependence. Since the cross sections for ^{148}Sm and ^{154}Sm were measured at the same laboratory bombarding energies, part of the deviation of the ratio from unity represents a trivial laboratory to center-of-mass transformation. This effect is rather small, however, and is shown by curve (c), which corresponds to the fusion of ^{16}O with fictitious spherical nuclei of the same radius but having masses 148 and 154.

Curve (b) isolates the effect of the volume change on the radius and is the ratio corresponding to fictitious spherical nuclei having identical masses but radii differing in the ratio $(154/148)^{1/3}$, i.e., differing by 1.3%. Curve (d), labeled by the measured values of β_λ, is the prediction to be compared with experiment. While producing good agreement at the higher bombarding energies (where the cross section is independent of deformation), it exceeds the measured ratio at low energies by nearly a factor of 3.

The expression for the change in radius with orientation given by Eq. (1) does not conserve the nuclear volume. To the order of terms in β^3, the radius R_t^0 must be decreased by an amount $R_t^0 \cdot (1/4\pi)\sum_\lambda \beta_\lambda^2$. This amounts to a decrease of 0.6% in the radius of ^{154}Sm which, when included in the calculation, yields curve (e) shown in Fig. 7. This correction produces a maximum change of only ~15% in the predicted cross section and thus is not the origin of the discrepancy.

One may question the assumption that the radius of the spherical potential used as a basis in these calculations actually increases as $A^{1/3}$; a less rapid rate of increase with neutron number would bring the prediction into better agreement with the data. There is evidence from isotope shift measurements[37] and from electron scattering[38] that the rms *charge* radius increases less rapidly than $A^{1/3}$—in fact, at about half this rate. This effect has an explanation in terms of an increase in the depth of the proton potential as neutrons are added, and thus does not require that the radius describing the mass distributions (to which the fusion cross section is sensitive) vary at a rate other than $A^{1/3}$. Even so, were the rms radius to vary as $A^{1/6}$, the predicted ratio at 60 MeV would be lowered by only 10%.

The calculation of the ratio $\sigma_{fus}(154)/\sigma_{fus}(148)$ with the known values of β_λ shows little sensitivity to whichever of the potentials in Table I is used. This may be understood from Fig. 6, which shows a decreasing relative sensitivity of the deduced value of β to the spherical potential used, once β becomes large ($\gtrsim 0.2$).

In the proximity formulation for the potential energy describing the interaction of heavy ions, the strength of the real potential is proportional to a generalized radius of curvature at the point where the gently curved surfaces of the nuclei come into contact.[24] Since the radius of curvature of a deformed nucleus is by definition not constant, the factor V_0 in Eq. (2) acquires an angular dependence as well.[39,40] Furthermore, as may be seen by an inspection of the inset in Fig. 3, the shortest distance of separation between projectile and target is no longer (because of the finite size of the projectile) along the line joining the centers of the nuclei. Both these effects have been considered by Randrup and Vaagen[39] for the case of ^{16}O + ^{168}Er. Because of the similar deformations of the nuclei ^{168}Er and ^{154}Sm, their results are directly applicable to our case. The effect of the angular dependence of the radius of curvature is to reduce the strength of the real potential at values of $\theta < 45°$, i.e., at angles for which the shift in radius associated with deformation would increase the strength of the potential for a given separation of the centers. Thus, this effect by itself should improve the agreement with experiment and does indeed, as shown by curve (a) in Fig. 8. However, the effect of the finite size of the projectile is to increase the strength of the potential (for a given separation and orientation), and when this is included as well, curve (b) is obtained. Thus, the inclusion of the additional angle-dependent terms for the nuclear potential does not, on the whole, improve the agreement between theory and experiment and, in fact, introduces an additional discrepancy at the high bombarding energies (see Fig. 8). This is not to suggest that these angle-dependent effects are not present, however, since there may be other problems with the basic equivalent-spheres approximation.

In order to check whether the discrepancy between theory and experiment might arise from some feature of the present analysis which involves integration of the Schrödinger equation for a complex potential, an analysis was undertaken

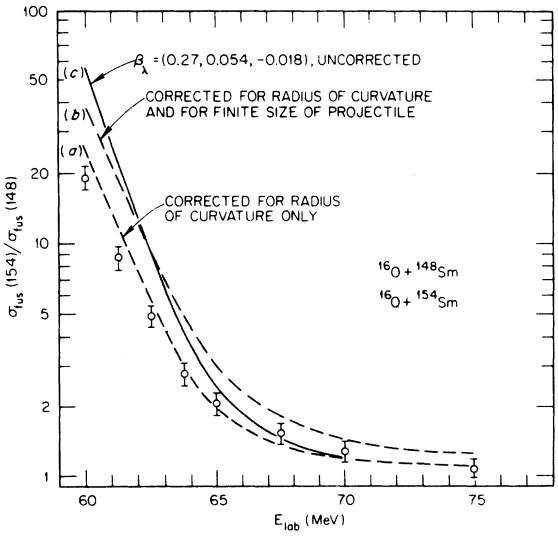

FIG. 8. Predictions of $\sigma_{fus}(154)/\sigma_{fus}(148)$ which take into account the "second-order" dependence of the real potential on the local radius of curvature and on the finite size of the projectile (Ref. 39).

using the "inverted parabola" approximation for the barrier. In this case, there is no imaginary potential and the transmission coefficients are given simply by the Hill-Wheeler expression.[7] The procedure was to search for a Woods-Saxon real nuclear potential that would reproduce the $^{16}O+^{148}Sm$ data when the combined Coulomb, nuclear, and centrifugal potentials were approximated by an inverted parabola. In this manner, deformation could then be introduced via the Woods-Saxon form factor. It was not possible to fit the entire range of the excitation function for $^{16}O+^{148}Sm$ with a single potential. Since three or four adjacent data points could be fit very well, however, an energy-dependent potential was introduced. When this was done, the ratio $\sigma_{fus}(154)/\sigma_{fus}(148)$ calculated for the known deformation parameters was very close to curve (d) in Fig. 7. This suggests that any calculational procedure using a particular real potential or complex potential will produce the same results for $^{16}O+^{154}Sm$, provided that this procedure reproduces the experimental data for $^{16}O+^{148}Sm$. This can be understood by writing

$$\frac{d\sigma}{d\beta}=\frac{d\sigma}{dE_B}\frac{dE_B}{d\beta}$$

and identifying $d\sigma/dE_B$ with the change in cross section for a small change in bombarding energy and $dE_B/d\beta$ with the change in an effective barrier height produced by a small change in deformation. The differential ratio $d\sigma/dE_B$ is very large, extremely sensitive to the choice of the spherical potential, and varies rapidly with bombarding energy. The ratio $dE_B/d\beta$ is small, not very sensitive (within reason) to the particular choice of the spherical potential, and is independent of bombarding energy. Forcing any calculation to fit the data for $^{16}O+^{148}Sm$ guarantees that the quantity $d\sigma/dE_B$ will be the same in all cases, and it is this fact that is responsible for the equivalent results obtained for the parabolic approximation (with an energy-dependent potential) and the Schrödinger equation plus a complex potential. We conclude from the above that the failure to reproduce the experimental data must rest with more fundamental aspects of the equivalent-spheres method.

There are several approximations made in the equivalent-spheres treatment that may affect the results in a significant way. The first of these may be called the "head-on" approximation. The specification of the orientation of the deformed nucleus only in terms of a polar angle [Eq. (1)] is equivalent to the assumption that all collisions are central, i.e., correspond to an orbital angular momentum $l=0$. Since the centrifugal barrier cannot be neglected in the barrier-penetration problem, finite impact parameters have been considered by the addition of the usual centrifugal potential $\hbar^2 l(l+1)/2\mu r^2$ for the collision of two point masses. However, this does not eliminate the need for an additional coordinate, an azimuthal angle, to specify the separation of the nuclear surfaces for finite impact parameters. If we define $\sigma_l=\pi\lambda^2(2l+1)T_l$, where T_l is the fusion transmission coefficient, then the l values for which $\sigma_l=\frac{1}{2}\sigma_l(\max)$ are $l=10$ and 20 at 60- and 70-MeV lab bombarding energies, respectively. Equating an impact parameter $b=l/k$, where k is the wave number, we have $b/R=0.2$ at 60 MeV and 0.4 at 70 MeV for $^{16}O+^{148}Sm$. As expected, the head-on approximation is more appropriate, the lower the bombarding energy.

Another assumption has been that the diffusivity of the nuclear potential is the same on all points of the nuclear surface. Since there is no *a priori* reason to doubt this assumption, it does not seem worthwhile to introduce additional (and *ad hoc*) free parameters to describe this effect.

As noted earlier, the vibration of the nuclear surface through quadrupole oscillations in the ground state (zero point motion) and excited states has not been treated properly in the present calculations which consider only static, permanent deformations. Since the amplitudes of the vibrational motion may be calculated from the known properties of the low-lying levels, it should be possible to include these effects without the introduction of additional free parameters.[36,41]

All of the foregoing calculations employ a static approximation, viz., that the deformation, excitation, and orientation of the target nucleus do not change as the projectile approaches. Dynamic effects will be considered in Secs. IV and V.

III. CALCULATIONS WITH A SINGLE AVERAGED SPHERICAL POTENTIAL

It is of interest to ask what results are obtained if, instead of averaging the cross sections calculated for potentials corresponding to different orientations as in Eq. (7), the potential itself is first averaged over all orientations and a fusion cross section then calculated. The potentials are averaged in the same way as the fusion cross section, i.e.,

$$\bar{V}(r,\beta),\bar{W}(r,\beta)=\int_0^{\pi/2}V(r,\beta,\theta),W(r,\beta,\theta)\sin\theta\,d\theta\,. \tag{8}$$

The radial forms of the resultant potentials are shown in Fig. 2. The ratio for fusion with ^{154}Sm and ^{148}Sm calculated with these potentials is shown by curve (a) in Fig. 9. Comparison of curves (b) and (c), for which only the imaginary potential and then

only the real potential were averaged, respectively, indicates that the gross discrepancy at high energies is associated with the imaginary potential. The averaging procedure in this case simply makes the nucleus appear too large [see Fig. 2(a)].

Another method of effectively taking an average before calculating the cross section is to use spherical potentials in which the radii (for the real and imaginary potentials) have been scaled not as $A^{1/3}$ but by the ratio of the half-density radii as determined by elastic electron scattering. The increase in radius for ^{154}Sm is, in this case, twice the increase given by an $A^{1/3}$ scaling and represents the effect of deformation. Such a procedure results in a ratio at 60-MeV lab, which is about 60% of the measured value. This and the results shown in Fig. 9 demonstrate that averaging the potential in the manner given by Eq. (8) is not a correct way to treat the effect of deformation in a static calculation. Indeed, elementary comparisons of a rotational or vibrational period and the collision time indicate that it is the cross section which should be averaged.

IV. CLASSICAL DYNAMICAL EFFECTS

The nucleus may undergo a change in shape and in orientation during the collision. As a result of this, the separation of the nuclear surfaces of target and projectile will be increased and some kinetic energy of relative motion will be converted into rotational energy and/or energy of deformation. These particular dynamic processes cause a reduction in the cross section for fusion or, equivalently, an increase in the barrier for fusion. Such effects have been considered by a number of authors for much heavier systems than the one studied here and were found to be small.[4,6]

Classical calculations of the collision of 60-MeV ^{16}O with ^{154}Sm have been performed by Levit[42] for a central collision. A value of 6.6 eb ($\beta_2 \approx 0.33$) was assumed for the intrinsic quadrupole moment of ^{154}Sm. Figure 10(a) shows the amount of angular momentum transferred to the target by the time the projectile has reached its distance of closet approach as a function of the initial angle of orientation. Taking the maximum value of $2.5\hbar$

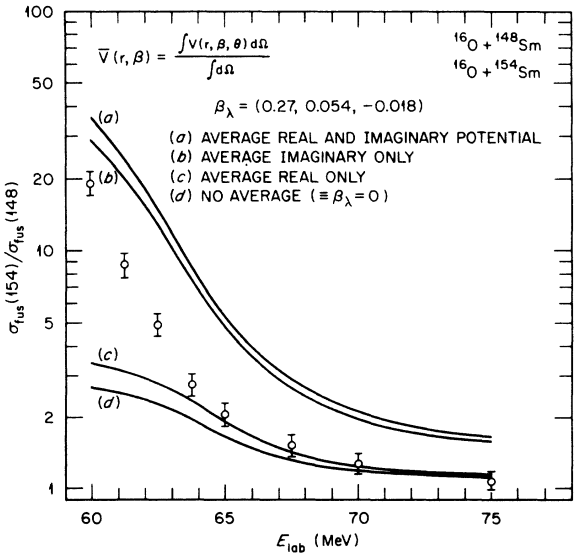

FIG. 9. Predictions in which the deformed potential is averaged over all orientations before calculating the fusion cross section.

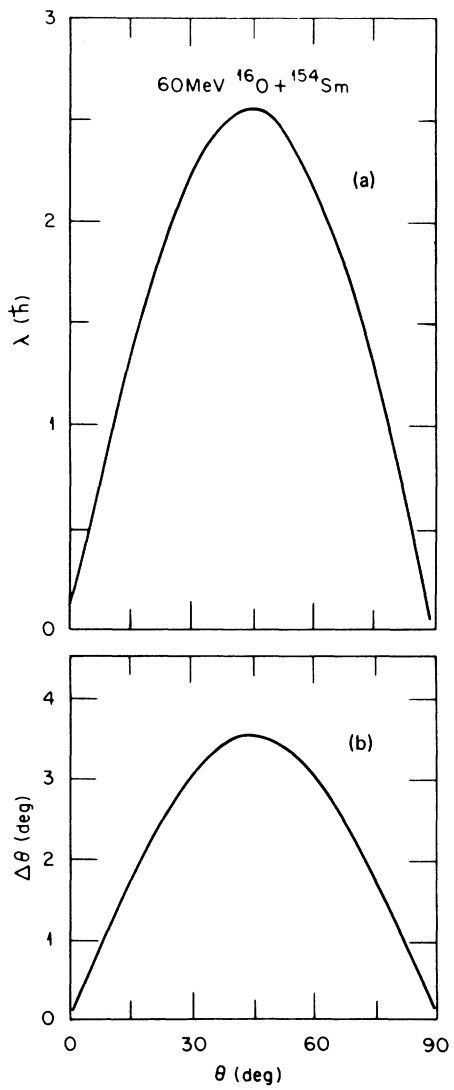

FIG. 10. Classical dynamical calculations of the angular momentum λ (a) and angle of rotation $\Delta\theta$ (b) attained by the deformed nucleus by the time the projectile has reached the distance of closest approach in a head-on collision (Ref. 42).

implies that an upper limit of ≈130 keV of kinetic energy is lost to rotation. Raising the barrier or lowering the bombarding energy by 130 keV c.m. results in an 11% decrease in the cross section. The amount of rotation undergone by the target when the projectile has reached the distance of closest approach is shown in Fig. 10(b). The effect of this on the cross section is calculated by shifting the curve $\sigma(\theta)\sin\theta$ by an amount appropriate for each initial orientation. This produces the dashed curve shown in Fig. 4 and a 32% reduction in the cross section. The combined result is a reduction by a factor of 1.5 in the predicted fusion cross section for 60-MeV $^{16}O+^{154}Sm$ and thus, *by itself*, can account for about half the discrepancy shown in Fig. 7.

Dynamical effects should be present for both the rotational nucleus ^{154}Sm and the vibrational nucleus ^{148}Sm; however, the relative sizes of these effects for the two nuclei will determine whether the prediction shown in Fig. 7 is brought into better agreement with experiment. It would be of value to have classical dynamical calculations of the type performed by Riesenfeldt and Thomas[6] for vibrational motion since these, together with calculations of the dynamic effects of rotation as described above, could answer this question.

V. COUPLED-CHANNELS CALCULATIONS

Both the statics and the dynamics of the fusion of nuclei having deformed equilibrium shapes are included in a coupled-channels treatment of the reaction. In such a treatment, inelastic excitations are considered explicitly through the inclusion of specific levels in the calculation, while the imaginary potential then represents all other inelastic processes, including fusion. Two different procedures are followed in comparing the results of these calculations to the data. The first comparison (a) is in complete analogy to the foregoing analyses. Thus, the same empirical spherical potential for which the calculated σ_R reproduces the fusion of $^{16}O+^{148}Sm$ ($\beta=0$) will be used to predict the fusion cross section for ^{154}Sm ($\beta\neq 0$) with the definition

$$\sigma_{fus}\equiv\sigma_R-\sigma_{2^+}-\sigma_{4^+}\,.$$

The second comparison (b) will use optical potentials obtained from fits to measured elastic and inelastic scattering of ^{16}O by $^{148,152}Sm$ (Ref. 43).

The coupled-channels calculations were performed with the code ECIS[44] written by J. Raynal. Partial waves through $l=300$ and a radial integration out to $r=70$ fm in steps of 0.06 fm were found to give sufficient precision in the calculation of σ_{fus} which at low energies is the difference of large and nearly equal quantities, σ_R and σ_{2^+} and σ_{4^+}.

Procedure (a). Since ECIS uses Woods-Saxon form factors for both the real and the imaginary potentials, potential set (iv) in Table I was deduced by fitting σ_{fus} for $^{16}O+^{148}Sm$ assuming $\beta=0$ and equating the total reaction cross section σ_R with σ_{fus}. The resulting fit is indistinguishable from that shown in Fig.1 for parameter set (i). The radii of this spherical potential are then scaled as $(A_p^{1/3}+A_t^{1/3})$ and used, together with the experimental values of β_2 and β_4 (and the associated $E2$ and $E4$ matrix elements[45]), to calculate $\sigma_{fus}=\sigma_R-\sigma_{2^+}-\sigma_{4^+}$. The result, plotted as a ratio $\sigma_{fus}(154)/\sigma_{fus}(148)$, turns out to agree within 10% with the static calculation [Eq. (7), curve (d) in Fig. 7]. (Since the 6^+ state is not strongly excited relative to the 2^+ and 4^+ states, it seems that its inclusion in the calculation would not change the above result.) It is quite probable, however, that this remarkable agreement between the two calculations is fortuitous and therefore does not imply that dynamic effects, such as those estimated classically in the previous system, are correspondingly small. A comparison at 60 MeV of σ_{fus} calculated for a deformed ^{154}Sm nucleus, but with and without the coupling to the excited states, indicates that the dynamic aspects of the fusion process decrease the cross section from the static value by a factor of about 1.7. This compares favorable with the factor 1.5 estimated in Sec. IV.

Procedure (b). In the foregoing procedure, the real and imaginary potentials were chosen such that σ_R reproduces the fusion cross section for $^{16}O+^{148}Sm$ ($\beta=0$). Calculations of the elastic and inelastic scattering using these potentials, experimental values of β_2, β_4, and the associated rotational model matrix elements $M(E\lambda)$ would not reproduce the measured elastic and inelastic cross sections. Since precise experimental data for $^{16}O+^{148,152}Sm$ scattering are available,[43] it is of interest to determine the potentials which, in a coupled-channels analysis, fit the scattering. A comparison of the resulting values of $\sigma_R-\sigma_{2^+}-\sigma_{4^+}$ with σ_{fus} (experiment) will then give an indication of the extent to which fusion dominates the inelastic processes.

The fitting procedure began with an optical potential found to fit 70-MeV $^{12}C+Nd$ inelastic scattering[46] and $B(E2\uparrow)$ and $B(E4\uparrow)$ values from Coulomb excitation.[46,47] Nuclear deformation parameters were obtained from the $B(E\lambda)$ values by use of the rolling model[45] to relate the nuclear interaction surface, $R_N=r_0(A_1^{1/3}+A_2^{1/3})[1+\beta_2^N Y_{20}(\theta)+\beta_4^N Y_{40}(\theta)+\cdots]$, to the Coulomb charge surface of the target, $R_C=r_C A_2^{1/3}[1+\beta_2^C Y_{20}(\theta)+\beta_4^C Y_{40}(\theta)+\cdots]$. As the optical model parameters became better

defined by searching on the $^{16}O + ^{148,152}Sm$ data,[43] slight changes were made in the $B(E\lambda)$ values to obtain better fits to the inelastic data.

Final optical model parameters and $M(E\lambda)$ values are shown in Tables II and III, respectively. The corresponding fits to the 72-MeV ^{16}O data are shown in Fig. 11 for the ^{148}Sm target and Fig. 12 for the ^{152}Sm target. An attempt was made to find a common spherical optical potential for both targets but, as can been seen in Table II, we require a different imaginary potential for each target. A similar finding for ^{12}C inelastic scattering for Nd isotopes has previously been reported.[46] Evidently, the elastic and inelastic scattering of ^{16}O by the Sm isotopes (as ^{12}C by the Nd isotopes) cannot be described simply by different deformations of a common spherical potential.

The $M(E\uparrow)$ values found to fit the 72-MeV ^{16}O data (Table III) are consistent with previous Coulomb excitation measurements.[47,48] We found that $M(E4\uparrow)$ for ^{152}Sm was quite sensitive to the 4^+ cross section beyond 80° c.m. and this is illustrated in Fig. 12 for three values of β_4^C. Within this range of β_4^C values there is no noticeable change in the calculated 0^+ and 2^+ cross sections. Unfortunately, the 4^+ state of ^{148}Sm could not be separated from the 3^- state, and a β_4 value of zero was assumed. The predicted 4^+ cross section for ^{148}Sm shown in Fig. 12 arises solely from double $E2$ excitation.

Predictions of σ_R, σ_{2^+}, and σ_{4^+} can only be made at energies other than 72 MeV by assuming that the optical potentials given in Table II are energy independent. It would seem that this assumption should be rather good (for our purposes) over an energy range extending 5 MeV on either side of the fit point 72 MeV. Such predictions are shown in Figs. 13 and 14 for $^{16}O + ^{148}Sm$ and $^{16}O + ^{152}Sm$, respectively. In both cases, the quantity $\sigma_R - \sigma_{2^+} - \sigma_{4^+}$ exceeds the measured fusion cross section at all energies. Peripherial processes, such as deep inelastic scattering, quasielastic transfer reactions, and sub-Coulomb transfer, are expected to be responsible for this difference. Peripheral processes (excluding the excitation of the ground-state band) thus amount to ~40% (150–180 mb) of the fusion cross section at 75 MeV and decrease less rapidly than fusion as the bombarding energy is lowered. At the fusion barrier (~65 MeV lab) these two mechanisms are nearly equal, and at 60 MeV the peripheral processes can exceed the fusion cross section by an order of magnitude or more. This renders it difficult, if not impossible, to perform coupled-channels calculations which explicitly treat all the important channels, leaving fusion alone to be represented by the imaginary potential.

TABLE II. Volume absorption Woods-Saxon optical model parameters obtained from a 0^+-2^+-4^+ coupled-channels fit to 72-MeV ^{16}O scattering from $^{148,152}Sm$.

	V (MeV)	r_0 (fm)	a_0 (fm)	W (MeV)	r' (fm)	a' (fm)	r_C (fm)
^{148}Sm	20.0	1.34	0.57	20.0	1.34	0.36	1.25
^{152}Sm	20.0	1.34	0.57	34.0	1.34	0.36	1.25

TABLE III. Coulomb deformation parameters (for r_C = 1.25 fm) and corresponding $M(E\lambda)$ values found from the coupled-channels fit to 72-MeV ^{16}O scattering data (Ref. 43) (Figs. 11 and 12).

	β_2^C	β_4^C	$M(E2\uparrow)$ (eb)	$M(E4\uparrow)$ (e^2b^2)
^{148}Sm	0.13	0.0	0.882	0.037
^{152}Sm	0.25	0.048	1.894	0.354

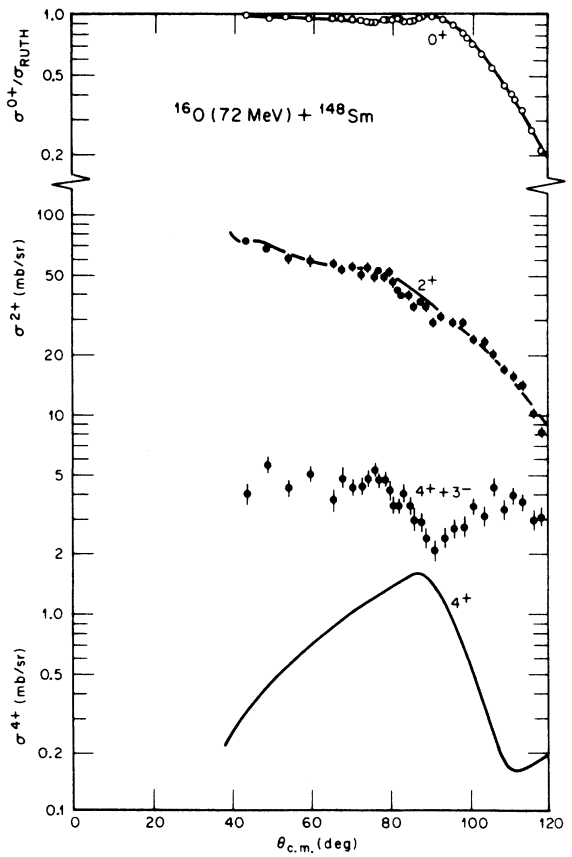

FIG. 11. Angular distributions for 72-MeV ^{16}O elastic (0^+) and inelastic scattering from ^{148}Sm (Ref. 43). The curves are the results of a $0^+ \leftrightarrow 2^+ \leftrightarrow 4^+$ rotational model calculation with the parameters of Tables II and III. The 3^- and 4^+ states were unresolved in the experiment.

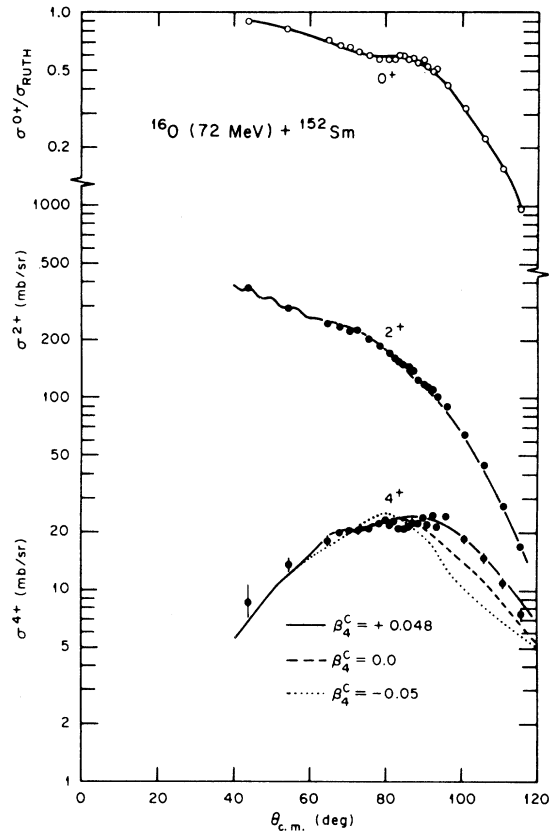

FIG. 12. Angular distributions for 72-MeV ^{16}O elastic (0$^+$) and inelastic scattering from ^{152}Sm (Ref. 43). The curves are the results of a 0$^+$ ⇔ 2$^+$ ⇔ 4$^+$ rotational model calculation with the parameters of Table II and Table III.

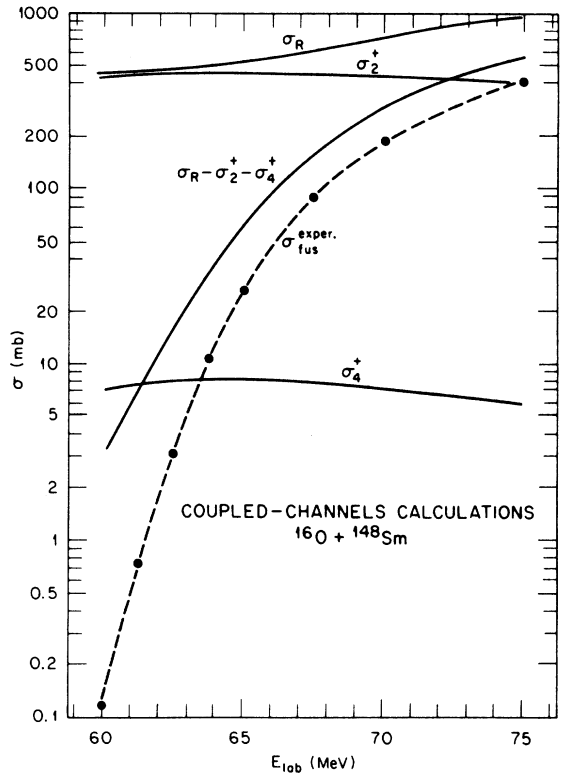

FIG. 13. Coupled-channels calculations σ_R, σ_{2^+}, σ_{4^+}, and $\sigma_R-\sigma_{2^+}-\sigma_{4^+}$ for ^{16}O+^{148}Sm using the parameters in Tables II and III. The potentials are assumed to be independent of bombarding energy.

VI. SUMMARY AND CONCLUSIONS

The availability of precise cross sections for sub-barrier fusion of ^{16}O with the isotopes of Sm has enabled a detailed examination of the current methods of calculating the effect of nuclear deformation on heavy-ion fusion. The approach was to adjust the undetermined parameters of the model (i.e., the potential) to fit the fusion cross sections for one isotope and use this information to make predictions for the other isotopes. Thus, it is mainly the differences in the observed cross sections that are of significance. The equivalent-spheres approximation, which considers the effect of static deformations, accounted for the trends in the data but overestimated the observed differences in the fusion cross sections for the different isotopes when known deformations were used. Equivalently, the deformations deduced from fitting the fusion data did not vary as widely with isotope number as those derived from $B(E2)$ values. A number of possible origins for this discrepancy were examined and most of them could be excluded. Remaining areas for further investigation include:

(i) the relaxation of the head-on approximation;
(ii) the inclusion of zero-point motion along with static deformation; and
(iii) further study of dynamic (i.e., coupled-channels) effects.

The calculations presented here (both classical and quantum mechanical estimates) suggest that these effects should not be neglected in comparing the fusion cross sections for vibrational and rotational nuclei. While most of the observed differences can be understood in terms of static deformation, the level of comparison with the data is now sufficiently precise that the dynamic effects could account for as much as half of the remaining discrepancy.

One technical problem with the coupled-channel analysis is, of course, the amount of computer time required. Further improvements in this area would allow coupled-channels fits to the fusion data.

Recent analyses of fusion data with heavier projectiles indicate that more than one dimension (the separation of the nuclei) may be required to ade-

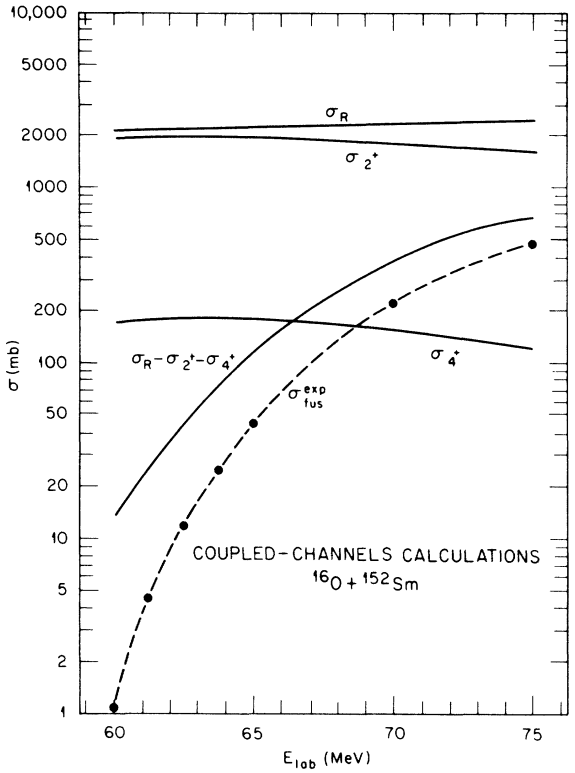

FIG. 14. Same as Fig. 13, but for $^{16}O+^{152}Sm$.

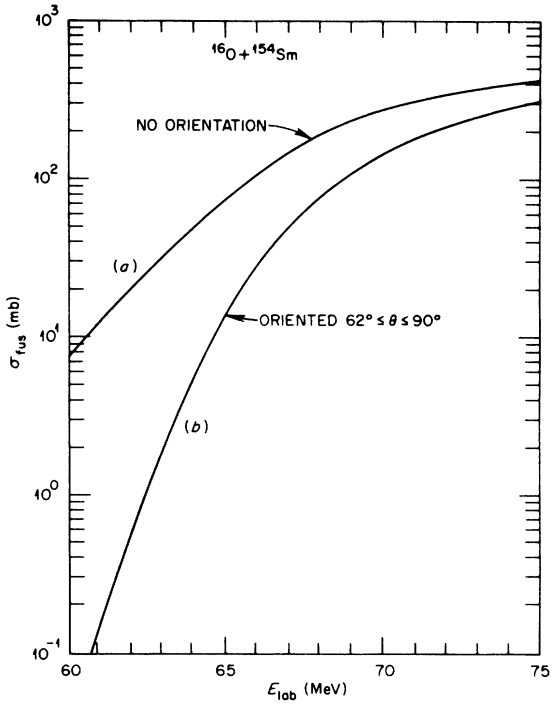

FIG. 15. An estimate of the variation in σ_{fus} for the case of an unpolarized ^{154}Sm target and a (hypothetical) ^{154}Sm target whose axis of symmetry was confined to angles between 62° and 90° with respect to the beam. Such a situation might be realizable with a polarized ^{160}Ho target (Ref. 52).

quately describe barrier penetration.[23,49-51] Throughout this analysis it has been assumed that the empirical adjustment of a potential to fit the data for one isotope effectively normalizes out for the other isotopes any effects which cannot be described by a one-dimensional potential. While there is no way at the moment to quantitatively check this assumption, it can only be noted that the assumption should be better the lighter the projectile.

In spite of the lack of success in obtaining precise agreement with the experimental data, it should be kept in mind that, once the challenging problems of understanding the reaction mechanism are better understood, sub-barrier fusion measurements offer interesting possibilities for the investigation of nuclear structure.

ACKNOWLEDGMENTS

We would like to thank S. Levit for several stimulating discussions and for performing the classical dynamical calculations. U. Smilansky and A. Baltz were most helpful during the early stages of the coupled-channels analysis. Several discussions with A. Winther, R. A. Broglia, and H. Esbensen on the topic of zero-point motion are gratefully acknowledged. Finally, we would like to thank N. Hintz for providing us with the experimental data on $^{16}O+^{148,152}Sm$ scattering. This work was sponsored in part by the Division of Basic Energy Sciences, U. S. Department of Energy, under Contract No. W-7405-eng-26 with the Union Carbide Corporation.

APPENDIX: FUSION MEASUREMENTS WITH A POLARIZED TARGET

Much of the sensitivity of the fusion cross section to deformation is lost because an average is made over all orientations of the deformed nucleus. In Fig. 4, $\sigma_{fus}(\theta)$ varies by a factor of ~4000 for a 90° change in orientation. After averaging over all angles, this change is reduced to a factor of 10 (see Fig. 5). Since it has been demonstrated that the deformed rare-earth nucleus ^{165}Ho can be polarized and that the polarization can be maintained in a scattering experiment,[52] it seems worthwhile to estimate the effects which might be expected in a fusion experiment. Since the deformations of ^{165}Ho and ^{154}Sm are similar, a calculation was performed in which $\sigma_{fus}(\theta)$ was averaged from 0° to 90° [curve (a), Fig. 15] and then from 62° to 90° [curve (b), Fig. 15]. The latter range of angles is

expected for a polarized ^{165}Ho target. Except for the averaging over a narrower range of angles, these calculations are the same as described for $^{16}O + ^{154}Sm$ and used to produce curve (d) in Fig. 7. As such, the predicted effect is probably overestimated; nevertheless, the calculations show that a strong variation in cross section is expected, and they may prove useful in planning an experiment.

---

*Present address: Lawrence Berkeley Laboratory, Berkeley, California 94720.

[1]G. Breit, M. Hull, and R. L. Gluckstern, Phys. Rev. 87, 74 (1952).

[2]R. Beringer, Phys. Rev. Lett. 18, 1006 (1967).

[3]C. Y. Wong, Phys. Lett. 26B, 120 (1968).

[4]H. Holm, W. Scheid, and W. Greiner, Phys. Lett. 29B, 473 (1969).

[5]A. S. Jensen and C. Y. Wong, Phys. Rev. C 1, 1321 (1970).

[6]P. W. Riesenfeldt and T. D. Thomas, Phys. Rev. C 2, 711 (1970).

[7]D. L. Hill and J. A. Wheeler, Phys. Rev. 89, 1102 (1953).

[8]S. H. Hanauer, J. W. T. Dabbs, L. D. Roberts, and G. W. Parker, Phys. Rev. 124, 1512 (1961).

[9]M. Beckerman and M. Blann, Phys. Rev. Lett. 42, 156 (1979).

[10]J. O. Rasmussen and K. Sugawara-Tanabe, Nucl. Phys. A171, 497 (1971).

[11]Y. Le Beyec, M. Lefort, and A. Vigny, Phys. Rev. C 3, 1268 (1971).

[12]H. Gauvin, Y. Le Beyec, M. Lefort, and C. Deprun, Phys. Rev. Lett. 28, 697 (1972).

[13]C. Y. Wong, Phys. Lett. 42B, 186 (1972).

[14]C. Y. Wong, Phys. Rev. Lett. 31, 766 (1973).

[15]H. Freiesleben and J. Huizenga, Nucl. Phys. A224, 503 (1974).

[16]J. S. Lilley and M. Franey, Bull. Am. Phys. Soc. 18, 605 (1973).

[17]J. M. Alexander, L. C. Vaz, and S. Y. Lin, Phys. Rev. Lett. 33, 1487 (1974).

[18]W. Scobel, A. Mingerey, M. Blann, and H. H. Gutbrod, Phys. Rev. C 11, 1701 (1975).

[19]L. C. Vaz and J. M. Alexander, Phys. Rev. C 10, 464 (1974).

[20]L. C. Vaz and J. M. Alexander, Phys. Rev. C 18, 2152 (1978).

[21]D. J. Morrissey, W. Loveland, R. J. Otto, and G. T. Seaborg, Phys. Lett. 74B, 35 (1978).

[22]R. G. Stokstad, Y. Eisen, S. Kaplanis, D. Pelte, V. Smilansky, and I. Tserruya, Phys. Rev. Lett. 41, 465 (1978); Phys. Rev. C 21, 2427 (1980).

[23]R. G. Stokstad, W. Reisdorf, K. D. Hildenbrand, J. V. Kratz, G. Wirth, R. Lucas, and J. Poitou, Z. Phys. A 295, 269 (1980).

[24]J. Blocki, J. Randrup, W. J. Swiatecki, and C. F. Tsang, Ann. Phys. 105, 427 (1977).

[25]G. R. Satchler and W. G. Love, Phys. Lett. 65B, 415 (1976).

[26]P. R. Christensen and A. Winther, Phys. Lett. 65B, 19 (1976).

[27]R. Bass, Nucl. Phys. A231, 45 (1974).

[28]K. Alder and A. Winther, Nucl. Phys. A132, 1 (1969).

[29]D. L. Hendrie, N. K. Glendenning, B. G. Harvey, O. N. Jarvis, H. H. Duhm, J. Saudinos, and J. Mahoney, Phys. Lett. 26B, 127 (1968).

[30]N. K. Glendenning, D. L. Hendrie, and O. N. Jarvis, Phys. Lett. 26B, 131 (1968).

[31]W. Bruckner, D. Husar, D. Pelte, K. Traxel, M. Samuel, and V. Smilansky, Nucl. Phys. A231, 159 (1974).

[32]A. H. Shaw and J. S. Greenberg, Phys. Rev. C 10, 263 (1974).

[33]R. Engfer, H. Schneuwly, J. L. Vuilleumier, H. K. Walter, and A. Zehnder, At. Data. Nucl. Data Tables 14, 509 (1974).

[34]P. H. Stelson and L. Grodzins, Nucl. Data Sect. A 1, 21 (1965).

[35]S. Raman, W. T. Milner, C. W. Nestor, Jr., and P. H. Stelson, in *Proceedings of the International Conference on Nuclear Structure, Tokyo, 1977*, edited by T. Marumori (Physical Society of Japan, Tokyo, 1978), p. 79.

[36]H. Esbensen, A. Winther, R. A. Broglia, and C. H. Dasso, Phys. Rev. Lett. 41, 296 (1978).

[37]A. Bohr and B. R. Mottelson, *Nuclear Structure* (Benjamin, New York, 1969), Vol. I, p. 162.

[38]C. W. de Jager, H. de Vries, and C. de Vries, At. Data Nucl. Data Tables 14, 479 (1974).

[39]J. Randrup and J. S. Vaagen, Phys. Lett. 77B, 170 (1978).

[40]R. A. Broglia, C. H. Dasso, G. Pollarolo, and A. Winther, Phys. Rep. 48, 351 (1975).

[41]A. Winther, private communication.

[42]S. Levit, private communication.

[43]D. J. Weber, N. M. Hintz, D. Dehnhard, J. L. Certz, and V. Shkolvik, Nucl. Phys. (to be published).

[44]J. Raynal, private communication; T. Tamura, Rev. Mod. Phys. 37, 679 (1965).

[45]D. L. Hendrie, Phys. Rev. Lett. 31, 478 (1973).

[46]D. L. Hillis, E. E. Gross, D. C. Hensley, C. R. Bingham, F. T. Baker, and A. Scott, Phys. Rev. C 16, 1467 (1977).

[47]T. K. Saylor, J. X. Saladin, I. Y. Lee, and K. A. Erb, Phys. Lett. 42B, 51 (1972).

[48]R. M. Diamond, F. S. Stephens, K. Nakai, and R. Nordhagen, Phys. Rev. C 3, 344 (1971).

[49]B. Sikora, J. Bisplinghoff, W. Scobel, M. Beckerman, and M. Blann, Phys. Rev. C 20, 2219 (1979).

[50]T. Kodama, R. A. M. S. Nazareth, P. Moller, and J. R. Nix, Phys. Rev. C 17, 111 (1978).

[51]L. C. Vaz, J. M. Alexander, and G. R. Satchler, Phys. Rev. C (to be published).

[52]D. R. Parks, S. L. Tabor, B. B. Triplett, H. T. King, T. R. Fischer, and B. A. Watson, Phys. Rev. Lett. 29, 1264 (1972).